Science Bulletin xxx (xxxx) xxx

Contents lists available at ScienceDirect

Science Bulletin

journal homepage: www.elsevier.com/locate/scib

Article

ZIF-L membrane with a membrane-interlocked-support composite architecture for H_2/CO_2 separation

Kun Yang [a,c], Sulei Hu [b], Yujie Ban [a,e,*], Yingwu Zhou [a,c], Na Cao [a,c], Meng Zhao [a,c], Yifei Xiao [d], Weixue Li [b,d,e], Weishen Yang [a,c,*]

[a] State Key Laboratory of Catalysis, Dalian Institute of Chemical Physics, Chinese Academy of Sciences, Dalian 116023, China
[b] Hefei National Laboratory for Physical Sciences at the Microscale, University of Science and Technology of China, Hefei 230026, China
[c] University of Chinese Academy of Sciences, Beijing 100039, China
[d] Department of Chemical Physics, School of Chemistry and Materials Science, iCHeM, Chinese Academy of Sciences, Excellence Center for Nanoscience, University of Science and Technology of China, Hefei 230026, China
[e] Dalian National Laboratory for Clean Energy, Dalian 116023, China

ARTICLE INFO

Article history:
Received 31 March 2021
Received in revised form 27 April 2021
Accepted 6 May 2021
Available online xxxx

Keywords:
MOF membranes
Membrane-interlocked-support composite architecture
H_2/CO_2 separation
Interfacial assembly

ABSTRACT

Metal–organic framework (MOF) membranes hold great promise in energy-efficient chemical separations. The outstanding challenges of the microstructural design stem from (1) thinning of membranes to immensely reduce the mass-transfer resistance (for high permeances); (2) tuning of orientation to optimize the selective transport of gas molecules, and (3) reinforcement of intercrystalline structure to subside leakage through defective gaps (for high selectivity). Here, we propose the ZIF-L membrane that is completely confined into the voids of the alumina support through an interfacial assembly process, producing an appealing membrane-interlocked-support (MIS) composite architecture that meets the requirements of the microstructural design of MOF membranes. Consequently, the membranes show average H_2 permeances of above 4000 GPU and H_2/CO_2 separation factor (SF) of above 200, representing record-high separation performances of ZIF-L membranes and falling into the industrial target zone (H_2 permeance > 1000 GPU and H_2/CO_2 SF > 60). Furthermore, the ZIF-L membrane possessing the MIS composite architecture that is established with alumina particles as scaffolds shows mechanical stability, scraped repeatedly by a piece of silicon rubber causing no selectivity loss.

1. Introduction

Metal–organic frameworks (MOFs), constructed through coordination between metal units and organic linkers, possess intrinsically porous backbones and exceptionally component diversities. The great promise these materials hold in various applications stems from their uniform arrangement of cavities (or portals) at molecular dimension [1–5]. Accordingly, as a novel type of crystalline molecular sieves, MOF membranes provide an energy-efficient method for gas separations, typified with the H_2/CO_2 separation that gains a growing prominence for a clean-energy and low-carbon future [6–11].

High-purity H_2 is generally needed, because it is not only a feedstock in the chemical and petrochemical industries, but also a sustainable green energy carrier. However, impurities (e.g., CO_2) often exist in H_2 production [12]. Separating H_2 from CO_2 using MOF membranes is a challenging task, which relies on distinguishing the molecule size nuances between H_2 and CO_2 (kinetic diameter, dH$_2$ = 0.289 nm, dCO$_2$ = 0.33 nm, Δd = 0.041 nm). For such a H_2/CO_2 separation application, three criteria are of paramount importance in the design of MOF membranes: (i) stacking ultrathin membrane layers that give rise to high permeances for the target gas component [9,10], (ii) stacking oriented membrane layers that contribute to a deliberate arrangement of pore arrays useful for high-selective molecule sieving [7,13], and (iii) (more importantly) strengthening crystal boundaries to eliminate defective gaps that would sacrifice the separation selectivity [14–17].

Zeolitic imidazolate framework (ZIF)-L is a famous two-dimensional (2D) layered MOF composed of periodic lamina alignment along *c*-direction (Fig. 1a), concomitant with free linkers staying between laminae to stabilize the structure. ZIF-L is a good candidate for the membrane because it possesses two kinds of mass-transfer pathways, namely hexagon window-like apertures (~0.34 nm) within a layer and galleries (~0.397 nm irrespective of free linkers) [18] between layers. Interestingly, interlaminar

* Corresponding authors.
E-mail addresses: yjban@dicp.ac.cn (Y. Ban), yangws@dicp.ac.cn (W. Yang).

https://doi.org/10.1016/j.scib.2021.05.006
2095-9273/

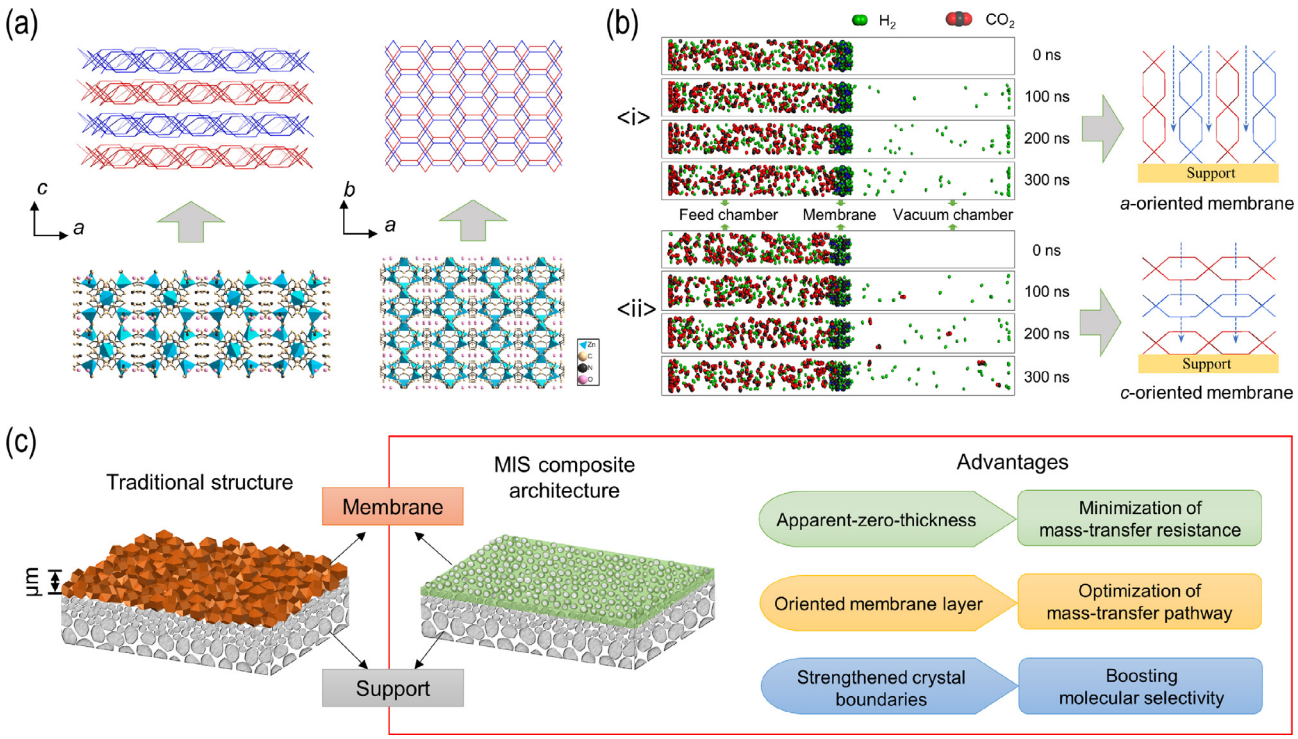

Fig. 1. Microstructural design of ZIF-L membranes. (a) Views of 2D layered crystal structure of ZIF-L along different directions and their wire-frame models connected by zinc nodes for simplicity. One wire represents a Zn-mim-Zn bond. (b) Simulation snapshots at 0, 100, 200 and 300 ns for H_2/CO_2 mixed gas molecules transporting through interlaminar galleries (panel i) or apertures within a layer (panel ii), and relevant orientation models of membranes. (c) Schematic representation of one MOF membrane with the traditional structure and MIS composite architecture.

galleries of 2D materials play a prominent role in molecular sieving of H_2 from CO_2, since abundant of guest molecules or functional groups aggregating between neighboring layers could hinder the diffusion of CO_2 in terms of interaction and render the effective interlaminar spacing a tighter fit for CO_2 [8,19–22]. Molecular dynamics (MD) simulations at hundreds-nanosecond (ns)-term are implemented in the current work to study the mixed-gas (H_2 and CO_2) transport through the two kinds of mass-transfer pathways of ZIF-L (Fig. 1b). It offers a direct proof that the passage of CO_2 through the interlaminar galleries faces a much larger barrier: the first passage for CO_2 through apertures within a layer is at 100 ns, whereas no CO_2 molecules are identified in the vacuum chamber even during 300-ns-long simulations (through interlaminar galleries). This result further proves a great molecular sieving potential of interlaminar galleries of ZIF-L in H_2/CO_2 separation. Accordingly, as shown in Fig. 1b, fabricating *a*-oriented (equivalent to *b*-oriented) ZIF-L membranes is a rational choice of making use of interlaminar cavities as an ideal molecular sieving pathway [23,24]. In addition, preliminary studies on ZIF-L crystal powder (leaf-like morphology, shown in Fig. 2) in our lab also demonstrated its near-zero coverage adsorption enthalpies (adsorption enthalpy at small gas loading) of H_2 and CO_2 are ~12 and ~33 kJ mol^{-1}, respectively (Fig. S1–S3 online). It means that 2D ZIF-L displays dramatic affinity to CO_2 over H_2 in thermodynamics, which might be due to interactions of uncoordinated nitrogen on the free linkers between laminae with CO_2 molecules [25]. The unique interaction could impede the transport of CO_2, which might provide a further boost for molecular sieving of H_2 from CO_2 through interlaminar galleries [19,21].

ZIF-L crystals featured with a shape of leaf-like nanosheet is a frequent building block for membranes [20,23,26–29]. As proved in previous literature, secondary growth of random nanocrystals based on Van der Drift mechanism [30] led to apparent-micrometer-thick ZIF-L membrane layers with undesirable stacking orientation on the surface of alumina support [23]. Wang and co-workers [23] also found that epitaxy growth of a flat deposition of ZIF-L nanosheets can induce the membrane orientation along *a*-axis and reduce the membrane thickness simultaneously. However, the membrane layer stacking on the surface of the support suffers from intercrystalline gaps, resulting in H_2/CO_2 separation selectivity for binary mixture of only 15.2. In brief, synthesis of MOF membranes with the separation performances exceeding the Robeson upper bound and falling into the industrial target zone (H_2 permeance > 1000 GPU, H_2/CO_2 selectivity > 60) [12] is challenging but urgently needed for practical purposes.

Here, we propose the ZIF-L membrane that is completely confined into the voids of the support through interfacial synthesis process, producing a membrane-interlocked-support (MIS) composite architecture to meet three criteria for microstructural design of MOF membranes, thus overcoming the abovementioned challenge (Fig. 1c). Compared with the traditional membrane structure, ZIF-L membrane with the MIS composite architecture is attractive owing to (1) apparent-zero-thickness that minimizes the mass-transfer resistance, (2) oriented establishment of the membrane with alumina particles as scaffolds in a constrained void space of a support, and (3) interlocked composites that correspond to strengthened crystal boundaries.

2. Experimental

2.1. Materials

Zinc nitrate hexahydrate ($Zn(NO_3)_2{\cdot}6H_2O$, Sigma-Aldrich, 99%), 2-methylimidazole ($C_4H_6N_2$, Sigma-Aldrich, 99%), and methanol (Sinopharm, AR) were used without further purification. Asymmetric α-Al_2O_3 disks (18 mm diameter, 1.0 mm thickness and 70 nm pores on the top layer) that were employed as supports were bought from Inocermic GmbH (Germany).

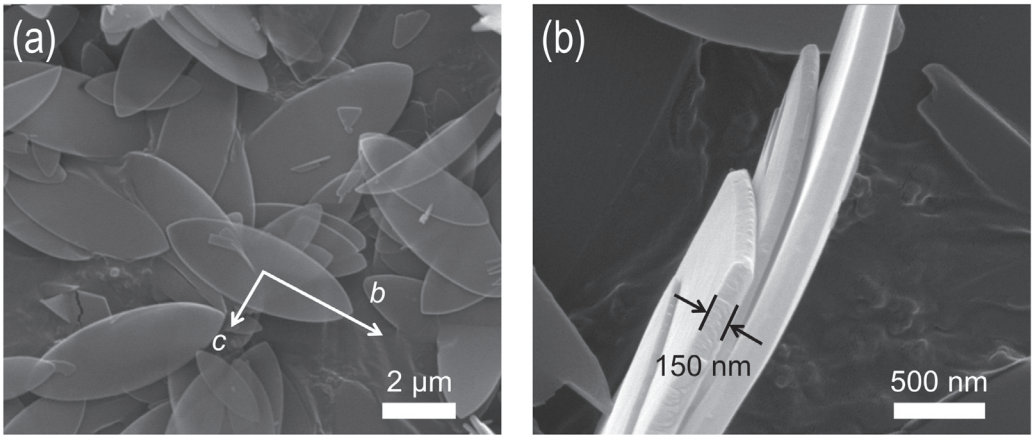

Fig. 2. (a) The typical leaf-like morphology of ZIF-L crystal powder. The out-of-plane axis is determined to be the *a*-axis [31]. (b) The thickness of ZIF-L nanosheets.

2.2. Preparations

2.2.1. Synthesis of ZIF-L crystal powders

ZIF-L crystals were synthesized according to the procedure reported by Wang and co-workers [25]. Typically, 0.59 g of Zn $(NO_3)_2{\cdot}6H_2O$ and 1.30 g of 2-methylimidazole (Hmim), dissolved in 40 mL of deionized (DI) water, respectively, were mixed under vigorous stirring at room temperature. The reaction lasted for 4 h. Then, the product was recovered through centrifugation, completely washed with DI water, and dried finally at 70 °C overnight.

2.2.2. Preparation of ZIF-L membranes

ZIF-L membranes were synthesized by the *in-situ* interfacial assembly (ISIA) method we developed previously after specific modifications [32]. A clean α-Al_2O_3 support was sealed into a home-designed noncorrosive-steel filter. Step 1: solid $Zn(NO_3)_2$ was dissoveld into 20 mL of methanol to form metal ion solution (2.95 g L^{-1}). With the help of a water pump, the solution was penetrated through the support, achieving metal ion injection into the support. Step 2: Hmim aqueous solution (approximate 20 mL) was decanted into the filter. Then, a gravity-driven permeation through the support was activated at a standard atmosphere. Metal-linker coordination reaction proceeded for 24 h at room temperature. After preparation, the membrane disk was removed from the filtration cell and washed with DI water. Then, the membranes were dried at 50 °C overnight. And membranes prepared at different concentrations of Hmim (65.0, 32.5, 6.50, 3.25, and 1.63 g L^{-1}) were marked as L1, L2, L3, L4, and L5, respectively.

2.3. Characterizations

The surface morphology of the ZIF-L membranes and powders were characterized by scanning electron microscopy (SEM, Quanta 200 FEG, FEI Co.) equipped with an energy-dispersive X-ray (EDX) detector. The X-ray diffraction (XRD) measurements were carried out on Rigaku D/MAX 2500/PC (radiation: Cu Kα, wavelength: 0.154 nm, accelerating voltage: 40 kV, current: 200 mA) at a scan speed of 5° min^{-1}. The patterns were collected at 2θ ranging from 3° to 40°. Thermogravimetric analysis (TG) was realized on a Netzsch device (STA 449F3). ZIF-L powder was heated from 40 to 800 °C with a rate of 10 °C min^{-1} under flowing air (20 mL min^{-1}). Gas adsorption was implemented on a integrated physisorption system (Micromeritics, ASAP 2020 Plus HD88) connected with a circulating bath.

2.4. Gas permeation experiments

ZIF-L membranes were sealed in a home-designed stainless-steel permeation cell. The gas separation performances based on W.-K. method were measured at room temperature. The feed flow rate was 100 mL min^{-1} (H_2: CO_2 = 1:1), and Ar (99.99%) was used as the sweep gas. Besides, separations based on different volumetric compositions of H_2/CO_2 as feed gas are also conducted. The concentration of penetrants was detected using a gas chromatograph (Agilent 7890B) equipped with a high sensitivity thermal conductivity detector (TCD).

The gas permeance was determined by Eq. (1):

$$P_i = \frac{N_i}{S\Delta p_i}, \tag{1}$$

where P_i (mol m^{-2} s^{-1} Pa^{-1}), N_i (mol s^{-1}) and $\triangle p_i$ (Pa) stand for the gas permeance, flow rate at standard conditions, and transmembrane pressure difference of component *i*, respectively. *S* (m^2) represents the effective membrane area. The gas permeance is commonly expressed in unit of GPU for simplicity. 1 GPU = 3.349 × 10^{-10} mol m^{-2} s^{-1} Pa^{-1}.

The separation factor was determined by Eq. (2):

$$\alpha_{ij} = \frac{P_i}{P_j}, \tag{2}$$

where P_i and P_j stands for the permeance of component *i* and component *j*, respectively.

Noted that the H_2 permeance and H_2/CO_2 separation factor of the bare α-Al_2O_3 disk are 29,000 GPU and 1.32, respectively.

2.5. Calculation of the orientation index (OI) for ZIF-L membrane

OI is calculated from the ratio of the two intensity factors (IF_{hkl}), as shown in Eq. (3):

$$OI = \frac{IF_{hkl,\,membrane}}{IF_{hkl,\,standard}}, \tag{3}$$

where IF_{hkl} is defined as the ratio of the intensity of the target diffraction peak to the sum of the intensities of the studied peaks, as shown in Eq. (4):

$$IF_{hkl} = \frac{I_{hkl}}{I_{hkl} + I_{h'k'l'} + I_{h''k''l''}}. \tag{4}$$

Noted that $IF_{standard}$ means the intensity factor of the powder sample synthesized in our lab.

2.6. Calculation of adsorption enthalpies (Q_{st})

The Clausius-Clapeyron equation was employed to calculate the experimental adsorption enthalpies (Q_{st}), as shown in Eq. (5):

$$Q_{st} = \frac{RT_1T_2 \ln(\frac{p_2}{p_1})}{T_2 - T_1}, \quad (5)$$

where p_1 (Pa) and p_2 (Pa) are the pressures reaching the same adsorption coverage at two temperatures T_1 (K) and T_2 (K), respectively. R stands for ideal gas constant (8.314 J mol^{-1} K^{-1}). In this study, Henry or Freundlich adsorption equations were selected to fit the isotherms (Fig. S3 online).

2.7. Water permeation experiments

The water permeation experiments were actualized by filtration processes. The ZIF-L membranes were sealed in a home-designed stainless-steel permeation cell. A certain volume of water was filtered through the membrane at the same time. The vacuum in the permeate side is maintained by a water pump, and the transmembrane pressure difference is approximate 1.0 bar.

The water permeance was determined by Eq. (6):

$$P = \frac{V}{\Delta pSt}, \quad (6)$$

where P is the water permeance, V represents the permeation volume of water though membranes, S is the effective membrane, t is the used time, and Δp is the transmembrane pressure difference.

2.8. MD simulations of the gas permeation through the MOF membrane

Simulation snapshots at 0, 100, 200, and 300 ns for the mixed-gas permeation systems (H_2 + CO_2) through *c*-oriented and *a*-oriented membrane, which is constructed by single cell in the selected direction (002) and (200), respectively. In the beginning (t = 0 ns), 129 H_2 and 129 CO_2 molecules were present in the feed chamber, which permeated through the MOF membrane to the evacuated permeate chamber.

Molecule dynamic simulation is performed using Dreiding force field [33], charge assignment method is based on Gasteiger-Marsili empirical atomic partial charges [34]. Time step is 0.1 ns. Simulation time duration is 300 ns. Temperature is 298 K. Ensemble is NVT. In total, the outputted number of frames are 3000 for each simulation. The density of mixed-gas permeation systems of H_2 and CO_2 is 0.2 g cm^{-3}. For the *c*-oriented membrane, the size of the simulation cell is 24.1171 Å× 17.0604 Å× 260 Å. For the *a*-oriented membrane, the size of the simulation cell is 17.0604 Å× 19.7398 Å× 260 Å.

3. Results and discussion

We select ceramic alumina disks as membrane supports. Fig. S4a (online) reveals the hierarchically cross-sectional structure of support that consists of a smooth ultrafiltration top layer and a microfiltration transition layer stacking on coarse particles. As described in Experimental Section, ISIA method developed in our lab was employed to synthesize ZIF-L membranes after specific modifications. The zinc ion solution (2.95 g L^{-1}) was first infiltrated through the alumina support with the aid of a water pump. Elemental mapping of the support after metal-ion injection, determined by SEM/EDS analysis (Fig. S4b and c online), shows a uniform distribution of Zn ions inside the alumina support instead of gathering on the top layer. The arrangement of reactive species at the interfacial domain of the support facilitates the formation of the membrane layer into the void of the support. Then, Hmim aqueous solution filtered through the support driven by gravity under a normal atmosphere, and engaged in a metal-linker coordinative reaction to form the membrane layer at room temperature.

XRD patterns of ZIF-L membranes synthesized at different concentrations of Hmim (Fig. 3) present a selective loss of diffraction peaks by comparison with that of isotropic ZIF-L crystal powder (Fig. S1 online), demonstrating that the control of micro-reaction at the interface leads to an evolution of preferred orientation of membranes. Specifically, the membrane synthesized at higher concentration of Hmim (65.0 g L^{-1}) shows a relatively strong XRD peak at 2θ of 9.1°, together with a weak peak at 2θ of 7.3°, which corresponds to (002) and (200) crystal planes along out-of-plane, respectively, according to diffraction geometry theory [35]. *OI* [36] is employed to quantitatively determine the predominant crystal planes with oriented arrangement. The *OI* value of (002) notably higher than that of (200) signifies the membrane with *c*-orientation (Fig. 3a). Decreasing the concentration of Hmim to 32.5 g L^{-1} gives rise to the membrane with the preservation of multiple XRD peaks (Fig. 3b), and leads to an increase of *OI* value of (200) planes but a decrease of that of (002) planes (Fig. 3b). A coexistence of crystal plane alignments is proved, and (200) crystal planes tend to develop at this condition. The membrane synthesized at 6.50 g L^{-1} of Hmim presents a (200) diffraction peak alone, suggesting a completely preferential orientation along *a*-axis (Fig. 3c).

We tentatively interpret the growth mechanism of the ZIF-L membrane based on the Van de Drift model. According to this theory, the orientation of MOF membranes is determined by the preferred growth direction of MOF crystals [37]. In the case of ZIF-L, the empirical growth rate along the *c* direction is much faster than that along the *a* direction. Thus, ZIF-L crystals display a leaf-like morphology (Fig. 2) [23]. As demonstrated in our previous study [32], ISIA process underpins the anisotropic growth of MOF membranes, and thereby controls the membrane orientation through the dynamics of metal-linker coordination at the interface. Consequently, the growth rate of ZIF-L along the *c* axis is strongly promoted by the high concentration of the linker but impeded by the diluted one. The latter case directly renders *a*-oriented growth dominant in the membrane.

SEM images further demonstrate the morphology evolution of ZIF-L membranes synthesized at different concentrations of the linker. The *c*-oriented membrane prepared at the higher concentration of Hmim (65.0 g L^{-1}) displays an extremely rough surface, appearing to take wrinkles that stick out from the support (typically marked with a dash rectangle, Fig. 3d). The apparent membrane thickness, determined by the discrete nanosheets from the cross-section, is around 40 nm (Fig. 3g). The development of (200) crystal planes with a decrease of the concentration of the linker make the membrane surface become smooth (from Fig. 3e to f), in particular for the complete *a*-oriented membrane (synthesized at 6.50 g L^{-1} of Hmim), which is as a result of the moderate reaction at the interfacial domain of the support. Specifically, this ultrathin membrane totally covers the support, with alumina particles clearly visible at the top surface of the support (Fig. 3f). From the cross-sectional image, the apparent thickness of the membrane apart from the surface of the support cannot be distinguished (Fig. 3i).

Further diluting the concentration of the linker solution (3.25 and 1.63 g L^{-1}) yields an extremely thin membrane that presents no signals in the XRD patterns. Both membranes display a similar microscopic morphology with the membrane synthesized at 6.50 g L^{-1} of Hmim, meaning that the orientation along *a*-axis is

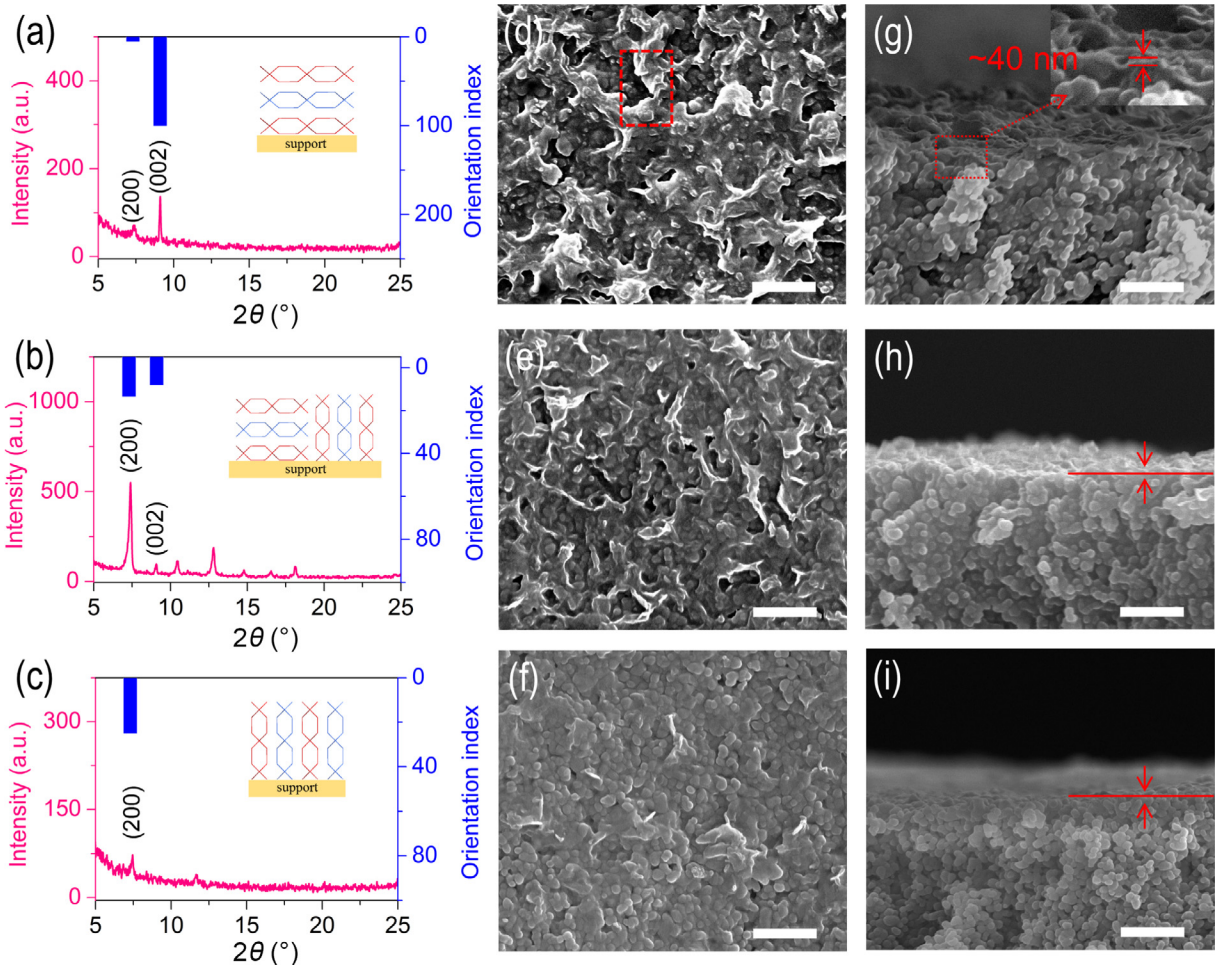

Fig. 3. Evolutionary orientation of ZIF-L membranes synthesized at the concentration of Hmim linker solution of 65.0 (a, d and g), 32.5 (b, e and h) and 6.50 g L^{-1} (c, f and i). (a–c) XRD patterns of ZIF-L membranes and orientation index of the specific crystal planes. (d–f) Top-surface and (g–i) cross-sectional SEM images of ZIF-L membranes (scale bars = 1 μm).

preserved. A discontinuity of the membrane layer appears on the top surface of the support, and the cross-sectional SEM image proves an apparent-zero-thick membrane (Fig. 4).

To demonstrate the compactness of the membranes above, we firstly conducted pressure-driven water permeation through the membranes synthesized at different concentrations of the linker (Fig. S5 online). Relative to water permeating directly through the bare support (790 L h^{-1} m^{-2} bar^{-1}), a notable mass-transfer resistance is revealed through the membranes, rendering water to vaporize under reduced pressure. A rough estimation of water permeance through membranes was determined by the loss of water owing to vaporization. The membrane synthesized at 65.0 g L^{-1} of Hmim (*c*-orientation) corresponds to a water permeance of ~1.35 L h^{-1} m^{-2} bar^{-1}. The development of the orientation along *a*-axis contributes to a densification of membranes. We find that the water permeance decreases by ~20% through the membrane synthesized at 6.50 g L^{-1} of Hmim (*a*-orientation). More interestingly, the membranes synthesized at very diluted linker solution (e.g., 3.25 and 1.63 g L^{-1}) appear to be rather discontinuous from the surface view of the support, but exhibit an exceeding compactness over other membranes. We speculate that in both cases the oriented membrane layer is confined into the voids of the support, forming a complete MIS composite architecture that shows apparent-zero-thickness apart from the surface of the support. Noted that the membranes synthesized at 65.0–6.50 g L^{-1} (from *c*-orientation to *a*-orientation) comprise of an ultrathin layer on the top surface of the support, and a partial MIS composite architecture.

To gain a deep insight of the intercrystalline structures (boundaries between crystals) of membranes, separation performances for equimolar H_2/CO_2 was conducted on ZIF-L membranes. Considering the reproducibility of membranes, Fig. 5a shows the average value with error bars of permeances and separation factors (SF) of membranes versus the synthetic concentrations of the linker. Expectedly, the membranes synthesized at 3.25 and 1.63 g L^{-1} of Hmim yield top average SF (H_2/CO_2) of 208 and 197, with average H_2 permeance of 4271 and 4843 GPU, respectively. The average value of performances cited from three synthetic groups (65.0, 6.50, 3.25 g L^{-1} of Hmim) is used to evaluate the enhancement of SF (H_2/CO_2), as shown in Fig. 5b. We find that tailoring the membrane from *c*-orientation to *a*-orientation only leads to a 2.1% enhancement of the average SF (H_2/CO_2), although the interlaminar transport pathways of ZIF-L membranes are thought to be desirable for separating H_2 from CO_2. The leakage through intercrystalline gaps arising from weak crystal-to-crystal connections would compromise the molecular sieving flow through the interlaminar pathways. Importantly, the intercrystalline structure (boundary between crystals) of the *a*-oriented membrane could be markedly strengthened as the complete MIS composite architecture generates. Membrane layers imbedded into such a constrained void space of the alumina support reveal a close linking between ZIF-L crystals, showing a SF enhancement above 91.5%.

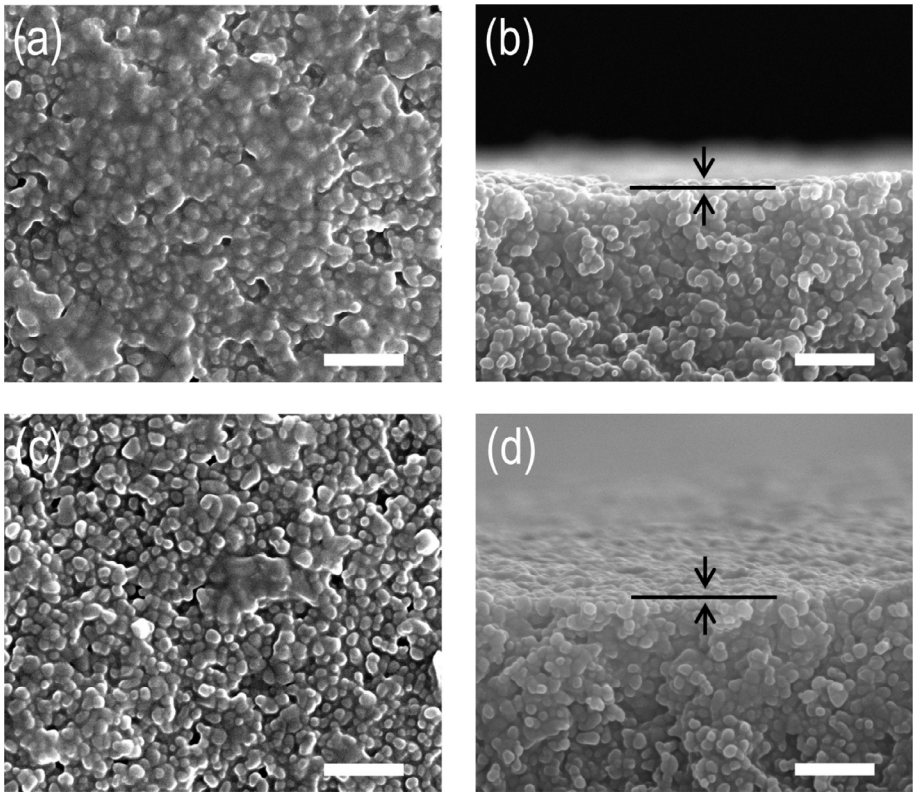

Fig. 4. Top-surface (a, c) and cross-sectional (b, d) SEM images of ZIF-L membranes synthesized at very diluted Hmim linker solution (3.25 g L^{-1} for (a, b) and 1.63 g L^{-1} for (c, d)). Scale bars = 1 μm.

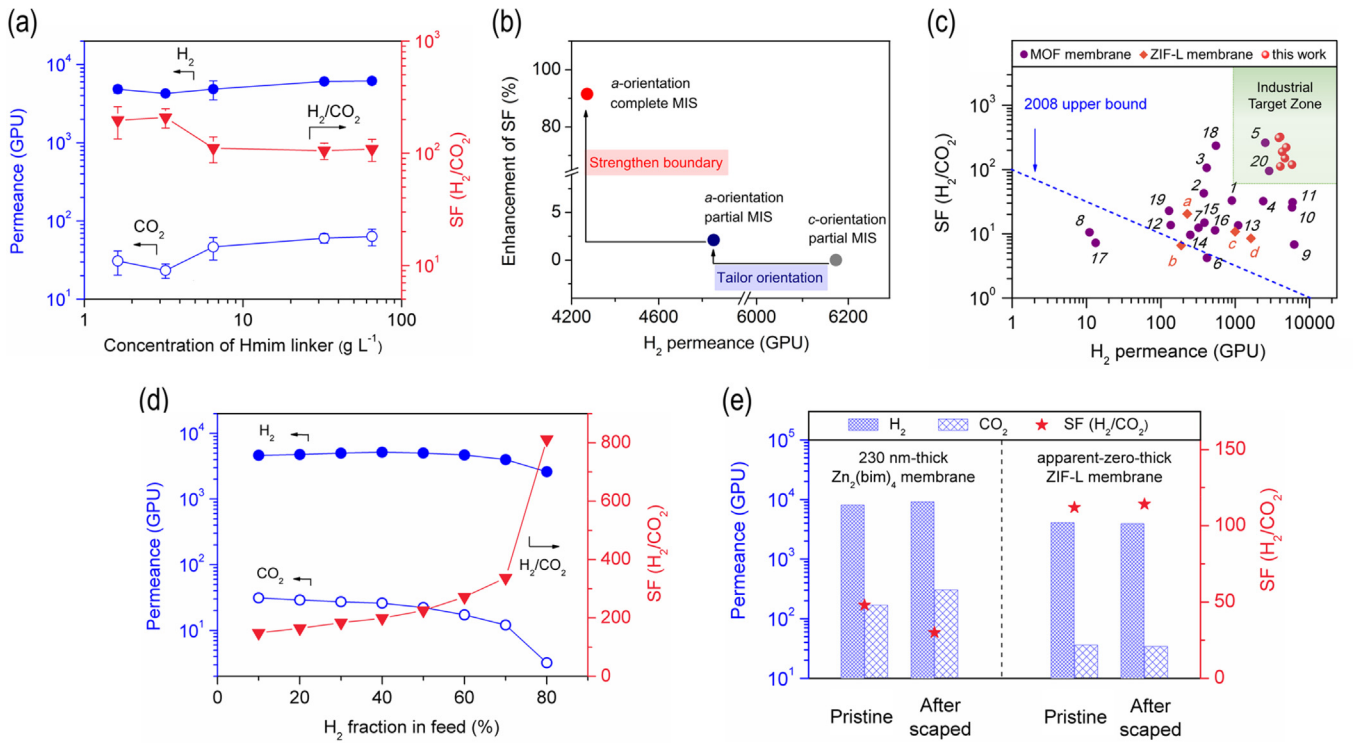

Fig. 5. Separation properties of ZIF-L membranes. (a) Average value with error bars of gas permeances and H_2/CO_2 SF of membranes versus the concentration of Hmim linker solution. (b) The enhancement of the average H_2/CO_2 SF of the membranes after tuning of the microstructures. (c) Comparison of separation performances of seven synthetic ZIF-L membranes with *a*-orientation and complete MIS composite architecture (red balls) in this work with previous ZIF-L membranes (orange symbols) and other MOF membranes (purple symbols) reported in literature. The data used here for comparison was also listed in Table S1 (online). For the Robeson's upper bound (2008), the permeability is converted to permeance assuming the membrane thickness of 0.1 μm. (d) The binary H_2/CO_2 separation performance of the ZIF-L membrane as a function of H_2 volume fraction in feed. (e) Gas permeances and H_2/CO_2 SF of the ZIF-L membrane after scaped.

Table 1
H_2 permeances and H_2/CO_2 SF of some typical MOF membranes under specific test conditions.

Membrane	Apparent thickness (nm)	Transmembrane pressure (bar) and temperature (K)	H_2 permeance (GPU)	SF H_2/CO_2	Ref.
$Zn_2(bim)_4$	5	0, 298	2700	291	[10]
ZIF-95	600	0, 298	2392	32.2	[7]
NH_2-MIL-53(Al)	~15,000	0, 298	5927	30.9	[38]
ZIF-L	5500	5, 298	1000	8.0[a]	[20]
ZIF-L	5000	0, 298	227	15.2	[23]
ZIF-L	2100	1, 298	1635	6.3	[28]
MIS-ZIF-L	~0	0, 298	4033	321	This work

a. Ideal selectivity determined from single gas permeations.

In comparison, seven synthetic ZIF-L membranes with *a*-orientation and complete MIS composite architecture (from 3.25 and 1.63 g L^{-1} of Hmim solution) in our study demonstrate remarkable H_2 permeances and SF of H_2 over CO_2, far above the Robeson's upper bound (2008) and falling into the industrial target zone (Fig. 5c and Table S1 online). Specifically, the optimal membrane shows H_2 permeance of 4033 GPU and SF (H_2/CO_2) of 321, surpassing the best value of H_2 permeance (2700 GPU) and SF (H_2/CO_2: 291) of $Zn_2(bim)_4$ nanosheet membranes (state-of-the-art MOF membranes) prepared from the top-down method (Table 1) [10]. Moreover, the appealing ZIF-L membrane manifests H_2/CO_2 SF approximate one order of magnitude higher than the MOF membranes that have H_2 permeances comparable to the current level (Table 1) [7,38]. Relative to other ZIF-L membranes in Refs. [20,23,28], ZIF-L membranes here present top separation performances for H_2/CO_2. The ZIF-L membrane cited from the optimal synthetical group (3.25 g L^{-1} of Hmim) also demonstrates excellent separation performances over a wide range of H_2 fraction in feed (Fig. 5d). SF of H_2/CO_2 reaches above 149 when the molar fraction of H_2 is only 10% in feed, which guarantees the efficiency in both of H_2-lean and H_2-rich separation processes. Additionally, different from the ultrathin $Zn_2(bim)_4$ membrane constructed by the ISIA method in our previous study [32], increasing temperature has slight effect on gas permeances of the ZIF-L membrane because of the compensation effect of the adsorption enthalpy for the activated permeation, providing nearly constant H_2/CO_2 SF under high temperature (Fig. S6 online), which is important for the practical separation.

In addition to benefits from separation performances, the membrane with complete MIS composite architecture is mechanically stable. The membrane layer is completely imbedded into the voids of the support instead of traditionally stacking on the surface of the support (Fig. 1c), ultimately developing into complete composites with alumina particles as scaffolds. Scraped repeatedly by a piece of silicon rubber, this apparent-zero-thick membrane is unwounded (constant gas permeances and SF; Fig. 5e), whereas another 230-nm-thick $Zn_2(bim)_4$ membrane prepared in our previous study [32], faces a dramatic loss of selectivity (~38%).

4. Conclusion

In summary, ZIF-L membranes that are completely imbedded into the voids of the alumina support were produced by the interfacial assembly method, showing apparent-zero-thickness apart from the surface of alumina supports. These membranes formed into the constrained void space present a complete membrane-interlocked-support (MIS) composite architecture, which is an optimal answer to the most important criteria for the microstructural design of membranes: ultrathin stacking membrane layers, orientation, close-knit crystal boundaries, and an unexpected abrasion resistance. The excellent breathability (~4271 GPU of average H_2 permeance) and selectivity (~208 of average H_2/CO_2 SF) of ZIF-L membranes is attractive to industry that need to cut down energy consumption and capital costs in processes. This study highlights the MIS composite structure that can be extended to other MOF membranes aiming for improving separation performances, and also proves the advances of the ISIA approach in controlling the microstructure of MOF membranes. Furthermore, we anticipate that the ISIA strategy demonstrated here will be modified in future to construct tubular and hollow fibber membranes that excel well in industry. Tuning of the metal-linker coordination reaction at the interface is likewise pivotal for these membranes.

Conflict of interest

The authors declare that they have no conflict of interest.

Author Contributions

Yujie Ban and Weishen Yang conceived and supervised the project. Yujie Ban and Kun Yang planned the experiments. Kun Yang prepared, characterized and tested membranes. Meng Zhao and Yingwu Zhou assisted the adsorption tests. Na Cao assisted the powder XRD characterization. Sulei Hu, Yifei Xiao and Weixue Li performed the simulation. Yujie Ban and Weishen Yang contributed to the data analysis, interpretation and Yujie Ban, Kun Yang and Weishen Yang wrote the paper.

Acknowledgments

This work was supported by the National Natural Science Foundation of China (21978283, 22090060, and 22090063), the Strategic Priority Research Program of Chinese Academy of Sciences (XDB17020400), Liaoning Revitalization Talents Program (XLYC1801004), the DNL Cooperation Fund, Chinese Academy of Sciences (DNL201920), Youth Innovation Promotion Association of Chinese Academy of Sciences, and Dalian Institute of Chemical Physics (DICP ZZBS201711). Weixue Li also thanks the financial support of National Key R&D Program of China (2018YFA0208603) and K.C. Wong Education Foundation (GJTD-2020-15).

Appendix A. Supplementary materials

Supplementary materials to this article can be found online at https://doi.org/10.1016/j.scib.2021.05.006.

References

[1] Furukawa H, Cordova KE, O'Keeffe M, et al. The chemistry and applications of metal–organic frameworks. Science 2013;341:1230444.
[2] Liao PQ, Huang NY, Zhang WX, et al. Controlling guest conformation for efficient purification of butadiene. Science 2017;356:1193–6.
[3] Uemura T, Yanai N, Kitagawa S. Polymerization reactions in porous coordination polymers. Chem Soc Rev 2009;38:1228–36.
[4] Gonzalez MI, Turkiewicz AB, Darago LE, et al. Confinement of atomically defined metal halide sheets in a metal–organic framework. Nature 2020;577:64–8.

[5] Li JR, Sculley J, Zhou HC. Metal–organic frameworks for separations. Chem Rev 2012;112:869–932.
[6] Cacho-Bailo F, Matito-Martos I, Perez-Carbajo J, et al. On the molecular mechanisms for the H_2/CO_2 separation performance of zeolite imidazolate framework two-layered membranes. Chem Sci 2017;8:325–33.
[7] Ma X, Wan Z, Li Y, et al. Anisotropic gas separation in oriented ZIF-95 membranes prepared by vapor-assisted in-plane epitaxial growth. Angew Chem Int Ed 2020;59:20858–62.
[8] Liu Y, Wang N, Pan JH, et al. *In situ* synthesis of MOF membranes on ZnAl-CO_3 LDH buffer layer-modified substrates. J Am Chem Soc 2014;136:14353–6.
[9] Wang X, Chi C, Zhang K, et al. Reversed thermo-switchable molecular sieving membranes composed of two-dimensional metal-organic nanosheets for gas separation. Nat Commun 2017;8:14460.
[10] Peng Y, Li Y, Ban Y, et al. Metal–organic framework nanosheets as building blocks for molecular sieving membranes. Science 2014;346:1356–9.
[11] Das S, Ben T, Qiu S, et al. Two-dimensional COF-three-dimensional MOF dual-layer membranes with unprecedentedly high H_2/CO_2 selectivity and ultrahigh gas permeabilities. ACS Appl Mater Interfaces 2020;12:52899–907.
[12] Ku AY, Kulkarni P, Shisler R, et al. Membrane performance requirements for carbon dioxide capture using hydrogen-selective membranes in integrated gasification combined cycle (IGCC) power plants. J Membr Sci 2011;367:233–9.
[13] Sun Y, Liu Y, Caro J, et al. In-plane epitaxial growth of highly *c*-oriented NH_2-MIL-125(Ti) membranes with superior H_2/CO_2 selectivity. Angew Chem Int Ed 2018;57:16088–93.
[14] Kwon HT, Jeong HK, Lee AS, et al. Heteroepitaxially grown zeolitic imidazolate framework membranes with unprecedented propylene/propane separation performances. J Am Chem Soc 2015;137:12304–11.
[15] Brown AJ, Brunelli NA, Eum K, et al. Interfacial microfluidic processing of metal–organic framework hollow fiber membranes. Science 2014;345:72–5.
[16] Ma XL, Kumar P, Mittal N, et al. Zeolitic imidazolate framework membranes made by ligand-induced permselectivation. Science 2018;361:1008–11.
[17] Choi J, Jeong HK, Snyder MA, et al. Grain boundary defect elimination in a zeolite membrane by rapid thermal processing. Science 2009;325:590–3.
[18] Low Z-X, Yao J, Liu Q, et al. Crystal transformation in zeolitic-imidazolate framework. Cryst Growth Des 2014;14:6589–98.
[19] Peng Y, Li Y, Ban Y, et al. Two-dimensional metal–organic framework nanosheets for membrane-based gas separation. Angew Chem Int Ed 2017;56:9757–61.
[20] Li H, Hou J, Bennett TD, et al. Templated growth of vertically aligned 2D metal–organic framework nanosheets. J Mater Chem A 2019;7:5811–8.
[21] Ding L, Wei Y, Li L, et al. MXene molecular sieving membranes for highly efficient gas separation. Nat Commun 2018;9:155.
[22] Wang Y, Liu B. Two-dimensional graphitic carbon nitride based membranes for separation. Sci Bull 2019;64:1385–7.
[23] Zhong Z, Yao J, Chen R, et al. Oriented two-dimensional zeolitic imidazolate framework-L membranes and their gas permeation properties. J Mater Chem A 2015;3:15715–22.
[24] Zhu J, Li H, Hou J, et al. Heteroepitaxial growth of vertically orientated zeolitic imidazolate framework-L (Co/Zn-ZIF-L) molecular sieve membranes. AIChE J 2020;66.
[25] Chen RZ, Yao JF, Gu QF, et al. A two-dimensional zeolitic imidazolate framework with a cushion-shaped cavity for CO_2 adsorption. Chem Commun 2013;49:9500–2.
[26] Lo Y, Kang D-Y. Pseudopolymorphic seeding for the rational synthesis of hybrid membranes with a zeolitic imidazolate framework for enhanced molecular separation performance. J Mater Chem A 2016;4:4172–9.
[27] Gu Q, Albert Ng TC, Sun Q, et al. Heterogeneous ZIF-L membranes with improved hydrophilicity and anti-bacterial adhesion for potential application in water treatment. RSC Adv 2019;9:1591–601.
[28] Wang S, Liu J, Pulido B, et al. Oriented zeolitic imidazolate framework (ZIF) nanocrystal films for molecular separation membranes. ACS Appl Nano Mater 2020;3:3839–46.
[29] Liang YY, Yu CJ, Ju JG, et al. Polymer-supported ultra-thin two-dimensional ZIF-L membranes through in-situ interface exfoliation for gas separation. Sci Bull 2020;65:1788–91.
[30] Vanderdrift A. Evolutionary selection a principle governing growth orientation in vapour-deposited layers. Philips Res Reports 1967;22:267–88.
[31] Conrad S, Kumar P, Xue F, et al. Controlling dissolution and transformation of zeolitic imidazolate frameworks by using electron-beam-induced amorphization. Angew Chem Int Ed 2018;57:13592–7.
[32] Yang K, Ban Y, Guo A, et al. *In-situ* interfacial assembly of ultra-H_2-permeable metal-organic framework membranes for H_2/CO_2 separation. J Membr Sci 2020;611.
[33] Mayo SL, Olafson BD, Goddard WA. Dreiding—a generic force-field for molecular simulations. J Phys Chem 1990;94:8897–909.
[34] Gasteiger J, Marsili M. A new model for calculating atomic charges in molecules. Tetrahedron Lett 1978;19:3181–4.
[35] Lai ZP, Bonilla G, Diaz I, et al. Microstructural optimization of a zeolite membrane for organic vapor separation. Science 2003;300:456–60.
[36] Hou Q, Zhou S, Wei Y, et al. Balancing the grain boundary structure and the framework flexibility through bimetallic metal–organic framework (MOF) membranes for gas separation. J Am Chem Soc 2020;142:9582–6.
[37] Li YS, Bux H, Feldhoff A, et al. Controllable synthesis of metal–organic frameworks: from MOF nanorods to oriented MOF membranes. Adv Mater 2010;22:3322–6.
[38] Zhang F, Zou X, Gao X, et al. Hydrogen selective NH_2-MIL-53(Al) MOF membranes with high permeability. Adv Funct Mater 2012;22:3583–90.

Kun Yang is currently a Ph.D. student in Physical Chemistry at Dalian Institute of Chemical Physics (DICP), Chinese Academy of Sciences (CAS). His research interest focuses on metal–organic framework membranes for gas separation.

Yujie Ban received her Ph.D. degree in Physical Chemistry from DICP, CAS in 2015, and worked as an Associate Professor at State Key Laboratory of Catalysis, DICP. Her research focuses mainly on metal–organic framework membranes, mixed matrix membranes, and novel porous networks for gas separation and liquid purification.

Weishen Yang received his Ph.D. degree from DICP, CAS in 1990. He has been a Full Professor of DICP, CAS since 1995. He devotes to the rational design and molecular-level engineering of functional nano-materials for applications in separation (e.g., zeolite membrane, metal–organic framework membrane, and mixed-conducting membrane) and in catalysis (e.g., catalytic conversion of C_1–C_4 alkanes).